nature communications

Article

https://doi.org/10.1038/s41467-025-60769-3

Orchestrating intratumoral DC-T cell immunity for enhanced tumor control via radiotherapy-activated TLR7/8 prodrugs in mice

Received: 4 September 2024

Accepted: 4 June 2025

Published online: 01 July 2025

Check for updates

Xiaozhe Yin[1,2,5], Zexuan Ding[3,5], Li Yu[1,2,5], Xuhao Zhang[1,2], Yu Gao[1,2], Yiyan Li[4], Zhibo Liu[3,4] ✉ & Yang-Xin Fu[1,2,3] ✉

Optimizing intratumoral dendritic cell (DC)-T cell responses is pivotal for effective cancer immunotherapy. However, the mechanistic governing these dynamics within the tumor microenvironment (TME) remains unclear, and strategies to improve their therapeutic potential are underexplored. Here, we show that precise radiotherapy activates the pro-TLR7/8 agonist imidazoquinoline (IMDQ) locally in preclinical tumor models, stimulating DCs to elicit T cell immunity without the need for further recruitment or causing systemic toxicity. Mechanistically, this synergistic approach triggers type I interferon via STING and MyD88 signaling pathways, strengthening local immune responses. Importantly, we reveal that fractionated, low-dose radiotherapy can effectively optimize local DC-T cell dynamics to control the irradiated tumor, while also promoting abscopal effect. Thus, our findings underscore the critical role of harnessing intratumoral DCs to reinvigorate pre-existing T cell immunity and provide mechanistic insights into improving both local and distal tumor control, opening new avenues for advancing cancer immunotherapy.

Activating the immune system to achieve therapeutic benefits in cancer treatment has long been a pursuit in the fields of immunology and oncology[1]. Dendritic cell (DC) serves as pivotal orchestrators of immune responses against tumors by priming T cell-mediated antitumor immunity[2,3]. Unlike the traditional view that draining lymph node (DLN) is the primary sites for immune activation against tumors, it is now recognized that substantial immune activity occurs within the tumor microenvironment (TME) itself[4–6]. However, it is not fully understood whether and how intratumoral DCs acquire and maintain their functional states to interact with T cells within the TME[6]. Targeting DCs selectively to rejuvenate TILs within the TME for local and distal tumors has proven challenging[7,8]. Moreover, the regulatory mechanisms that govern interactions between intratumoral DCs and T cells are not fully elucidated[7].

The abscopal effect represents a promising avenue for improving cancer treatment outcomes, which involves a complex interplay between radiation, DCs and T cells[9,10]. The localized radiation induces a systemic immune response with DCs presenting tumor antigens to T cells, which then attack not just the irradiated tumor but also distant tumors[11,12]. However, high doses of local radiation can effectively

[1]Department of Basic Medical Sciences, School of Medicine, Tsinghua University, Beijing 100084, China. [2]State Key laboratory of Molecular oncology, Tsinghua University, Beijing, China. [3]Changping Laboratory, Beijing 102206, China. [4]Beijing National Laboratory for Molecular Sciences, Radiochemistry and Radiation Chemistry Key Laboratory of Fundamental Science, Key Laboratory of Bioorganic Chemistry and Molecular Engineering of Ministry of Education, College of Chemistry and Molecular Engineering, Peking University, Beijing 100871, China. [5]These authors contributed equally: Xiaozhe Yin, Zexuan Ding, Li Yu. ✉e-mail: zbliu@pku.edu.cn; yangxinfu@tsinghua.edu.cn

control targeted tumor, but the abscopal effect are rare, due to the harmful impact on immune cells inside TME[13–16]. This highlights the need for innovative approaches that optimize DC-T cell dynamics locally while facilitating systemic immune effects[17–19]. Understanding how intratumoral DC-T cell interactions contribute to the abscopal effect may provide new strategies for enhancing cancer immunotherapy.

DC activation through Toll-like receptor 7/8 (TLR7/8) signaling has shown great potential in stimulating antitumor immunity[20]. TLR7/8 agonists robustly engage innate immune pathways, enhancing DC activation and subsequent T cell priming[21]. However, systemic delivery of these agonists has been limited by severe toxicities, emphasizing the need for strategies that maximize their local effects while minimizing systemic exposure[21,22]. Local delivery of TLR7/8 agonists has demonstrated efficacy in enhancing immune activity within the TME[23,24]. However, effective local delivery remains largely confined to superficial tumors due to issues such as rapid leakage post-delivery and uneven distribution within the TME[25,26].

Recent advancements have enabled the use of radiotherapy-induced chemical reactions to activate drugs, allowing for targeted drug delivery without systemic toxicity[27–30]. In our previous work, we developed a strategy to cage drugs using oxygen atoms[31]. Oxides can be effectively reduced by hydrated electrons (e^-_{aq}) generated from radiation[31,32]. Building on the radiotherapy-activated prodrug (RAP) strategy, we propose to enhance intratumoral immune activation by focusing on DC-T cell interactions within the TME. This method modifies the TLR7/8 agonist imidazoquinoline (IMDQ) by strategically installing a single oxygen atom to form *N*-oxide prodrugs and transiently blocking its receptor-binding activity. Subsequent local radiation of prodrug within the TME restores the full agonistic potential of the agonist, promoting tumor rejection without peripheral toxicity. By leveraging RAP to activate DCs locally, our study aims to elucidate the mechanisms governing intratumoral DC-T cell dynamics and their role in achieving local tumor control and systemic immune responses. Interestingly, our findings demonstrate that signals via STING and MyD88 regulate type I interferon (IFN) production, facilitating DC-mediated T cell activation against local and distal tumors. Our study addresses the challenge of enhancing intratumoral immune activation and deepening our understanding of DC-T cell responses within the TME.

Results

Local X-ray induces TLR7/8 agonist prodrug intratumoral activation

To achieve the potent TLR7/8 agonist IMDQ intratumoral activation without systemic toxicity, we employed the RAP technique, which involved introducing a single oxygen atom to the quinoline nitrogen atom through a straightforward *N*-oxidation reaction (Fig. 1a and Supplementary Figs. 1–4a). The N-heterocyclic structure of IMDQ interacts intricately with amino acid residues within the TLR8 pocket[33], particularly stabilizing TLR8 in its activated state through interactions with Thr574 and Asp543 (Supplementary Fig. 4b). However, the introduction of an oxygen atom in *O*-IMDQ disrupted the interaction, making it difficult to maintain the active dimeric structure. This alteration prevented them from being locked in an activated state (Supplementary Fig. 4b). Previous studies have demonstrated that X-ray-induced water radiolysis generated hydrated electrons (e^-_{aq})[34], known for their strong reducing capacity in aqueous solutions (Supplementary Fig. 4c). Consequently, X-ray-generated e^-_{aq} could efficiently activate oxygen atom-engineered immune agonist prodrugs through reduction (Supplementary Fig. 4d), thereby enabling prodrug responsiveness to X-ray radiation. To address the conversion of *O*-IMDQ to the parent drug IMDQ, we employed both HPLC and UPLC-MS analyses (Supplementary Figs. 5, 6). These results confirmed the release of IMDQ upon radiation treatment, providing strong evidence that *O*-IMDQ acts as a prodrug and is effectively converted into the active parent compound under irradiation conditions.

Next, we utilized RAW-blue and hTLR8 reporter cells to assess the blockade and restoration of *O*-IMDQ activity. Our findings demonstrated that the addition of a single oxygen atom effectively attenuated IMDQ's immunostimulatory activity, which was subsequently restored upon exposure to X-ray radiation (Fig. 1b, c). To confirm the regained potency of *O*-IMDQ after X-ray exposure, we generated bone marrow-derived dendritic cells (BMDCs) in vitro and evaluated their functional characteristics after activation with *O*-IMDQ. We observed that *O*-IMDQ did not compromise the upregulation of typical activation markers (CD80 and CD86) (Fig. 1d and Supplementary Fig. 7a) and cytokine secretion (TNF and IL12) (Supplementary Fig. 7b, c), and it also failed to enhance antigen presentation function (Fig. 1e), indicating the activity block of *O*-IMDQ. However, X-ray exposure significantly increased the upregulation of these factors, suggesting a functional restoration of *O*-IMDQ (Fig. 1d, e).

To assess the systemic safety of *O*-IMDQ administration in vivo, we monitored changes in mouse weight and tumor volume with varying doses of IMDQ and *O*-IMDQ in MC38 tumor-bearing mice. We observed that IMDQ induced weight loss, though it effectively promoted dose-dependent tumor regression. In contrast, single *O*-IMDQ showed no systemic toxicity and lacked antitumor effects (Fig. 1f, g). Furthermore, serum analysis revealed that *O*-IMDQ exhibited undetectable levels of inflammatory cytokines (MCP-1, TNF, IL-10, and IL-6) compared to IMDQ (Fig. 1h, i, and Supplementary Fig. 8a, b). We also analyzed the distribution of *O*-IMDQ in various organs and peripheral blood after intravenous administration. Our results show that, in the absence of radiation, IMDQ is detectable in various tissues, whereas *O*-IMDQ remains largely inactive, with no detectable levels of active IMDQ in any tissue, indicating no unintended activation without radiation (Supplementary Fig. 8c). The results of histopathological analyses across multiple organs further confirm that *O*-IMDQ does not induce detectable organ toxicity (Supplementary Fig. 8d). Additionally, detailed biochemical measurements, including aspartate aminotransferase (AST), alanine aminotransferase (ALT), and uric acid (UA) levels, demonstrate that the prodrug does not cause hepatic, renal and broad tissue toxicity (Supplementary Fig. 8e). These data provide a more rigorous and comprehensive assessment of the prodrug's safety profile, further supporting its potential for clinical application.

To further confirm intratumoral activation and optimize the therapeutic efficacy of *O*-IMDQ following radiation, we determined the optimal timing for radiation delivery. Based on the peak accumulation of *O*-IMDQ in tumors one hour after systemic administration (Supplementary Fig. 9a), we evaluated activation and the antitumor activity of *O*-IMDQ combined with radiotherapy (6 Gy) in an MC38 colon tumor model. Upon radiation treatment following intravenous administration, a significant accumulation of active IMDQ was observed only at the tumor site, confirming that the prodrug's activation is strictly radiation-dependent (Supplementary Fig. 9b). We also measured cytokine levels in different tissues 1 h post-irradiation. Our findings revealed that a substantial cytokine response was only detected in the tumor 1 h post-irradiation, with no significant cytokine elevation in other tissues, indicating an absence of systemic inflammatory reactions (Supplementary Fig. 9c). Additionally, to further substantiate these findings, we included an *O*-IMDQ-only control group in the tumor treatment experiments. The results indicate that *O*-IMDQ alone did not affect tumor growth, whereas the combination of *O*-IMDQ with radiation effectively controlled tumor progression without inducing body weight loss or organ toxicity (Fig. 1j, k and Supplementary Fig. 8d, e). Furthermore, in vivo experiments to test tumor-associated DC activation confirmed that *O*-IMDQ activation requires radiation exposure (Supplementary Fig. 9d, e). We also applied the same modification to other TLR7/8 agonists (R848 and BBIQ) and demonstrated the effectiveness of radiotherapy-induced

https://doi.org/10.1038/s41467-025-60769-3

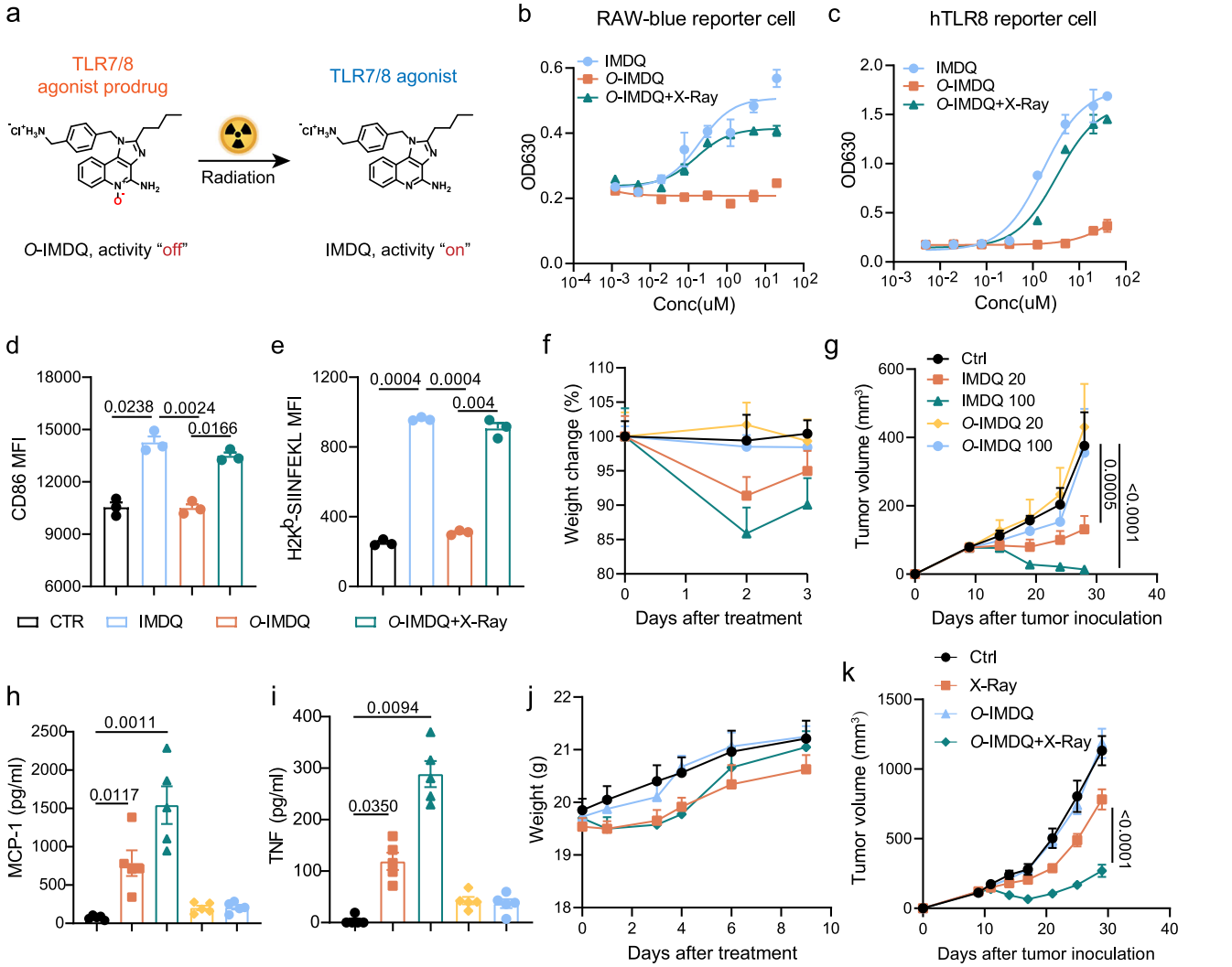

Fig. 1 | Local X-ray activates TLR7/8 agonist prodrug to control tumor. a The schematic diagram of *O*-IMDQ activity releasing. **b** TLR7/8 activation curves of IMDQ, *O*-IMDQ treated with or without X-Ray (10 Gy) in RAW-blue reporter cells after 24 h incubation ($n = 2$ cells, but technical replicates are three times.). **c** TLR7/8 activation curves of IMDQ, *O*-IMDQ treated with or without X-Ray (10 Gy) in hTLR8 reporter cells after 24 h incubation ($n = 2$ cells, but technical replicates are three times.). **d** BMDCs were stimulated with 1 μM IMDQ and *O*-IMDQ irradiated together by 10 Gy for 24 h. The activation marker was measured by flow cytometry ($n = 3$ cells). **e** BMDCs were stimulated with 1 μM IMDQ and *O*-IMDQ irradiated together by 10 Gy for 24 h. Antigen presentation was measured by flow cytometry ($n = 3$ cells). **f** MC38 tumor-bearing mice (6–8 weeks old female C57BL/6J mice) were treated with different doses (20 μg/mice and 100 μg/mice) IMDQ and *O*-IMDQ on day 10, 13, and 16. Body weight was measured ($n = 6$ mice). **g** Tumor growth was measured ($n = 6$ mice). **h** Serum was collected 24 h after the first injection. MCP-1 in serum was analyzed by cytometric bead assay ($n = 6$ mice). **i** TNF in serum was analyzed by cytometric bead assay ($n = 6$ mice). **j** MC38 tumor-bearing mice (6–8 weeks old female C57BL/6 J mice) were i.v. treated with *O*-IMDQ on days 10, 13, and 16. One hour later, mice were irradiated by 6 Gy or not. Body weight was measured ($n = 8$ mice). **k** Tumor growth was measured ($n = 8$ mice). Data were shown as mean ± SEM and are representative of at least three independent experiments. Statistical analysis was performed using Student's two-tailed unpaired *t*-test (**d**, **e**, **h**, **i**) or two-way ANOVA (**g**, **k**). Exact *P* value has been provided in the figures. *N* numbers define the biological replicates. Source data are provided as a Source Data file.

activation (Supplementary Fig. 13). These findings collectively demonstrate that *O*-IMDQ is selectively activated in the tumor upon radiation, thereby enhancing TLR7/8 signaling activation inside TME and promoting tumor rejection without peripheral toxicity.

cDC1s and pre-existing CD8$^+$ T cells are crucial for the antitumor efficacy of radiotherapy-activated *O*-IMDQ

To elucidate the role of local DC-T immunity responses in radiotherapy-activated *O*-IMDQ-mediated tumor control, we investigated the specific cellular mechanisms contributing to its therapeutic effects. Using targeted antibody depletion, we individually removed distinct subsets of immune cells or potential effector molecules to assess their impact. While TLR7/8 agonists are known to activate macrophages[35], macrophage depletion did not affect therapy outcomes (Fig. 2a, b). Similarly, depletion of NK cells or CD4 had no impact on therapy efficacy. However, depletion of CD8$^+$ T cells and neutralization of IFNγ completely abrogated the therapeutic effect (Fig. 2a–c), highlighting their essential roles. Upon activation by TLR7/8 agonist, DCs might migrate to DLNs where they prime T cells or directly reactivate local pre-existing T cells. To further determine whether radiotherapy-activated *O*-IMDQ treatment mainly depends on recruitment from LNs or pre-existing T cells within the TME, we administered FTY720 (a small-molecule analog of sphingosine 1-phosphate) to prevent T cell infiltration into the TME[36]. The therapeutic effect was impressively unaffected by administration of FTY720 (Fig. 2d). We also observed similar results in B16/F10 tumor model (Supplementary Fig. 10a). In our study, we also used FTY720 to prevent T cell trafficking to TME at different tumor stages and

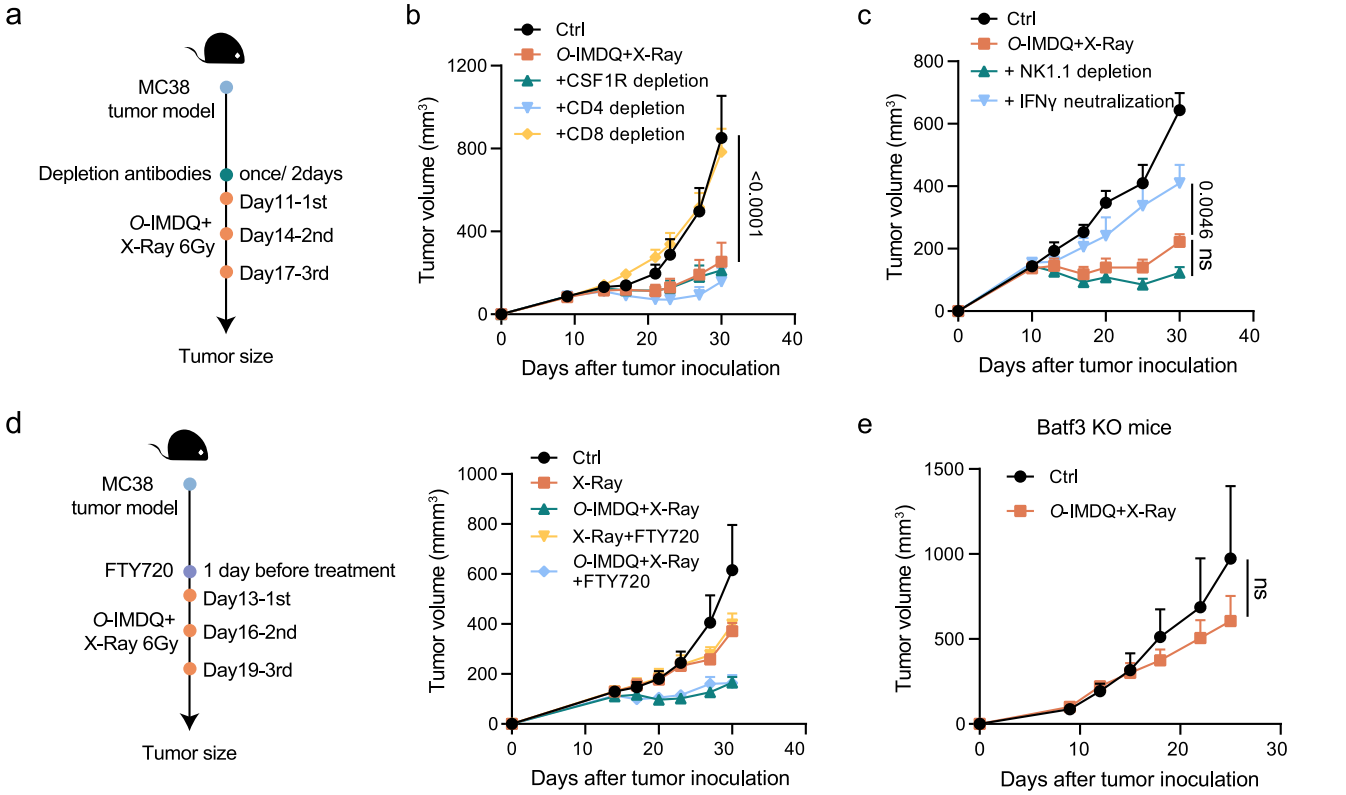

Fig. 2 | The antitumor effect of radiotherapy-activated *O*-IMDQ depends on cDC1 and pre-existing CD8⁺ T cells. a The schematic of radiotherapy-activated TLR7/8 agonist treatment. **b** MC38 tumor-bearing mice (6–8 weeks old female C57BL/6J mice) were treated as (**a**). For cell depletion, mice were injected with 500 μg anti-CSF1R Ab or 200 μg anti-CD4 Ab or 200 μg anti-CD8 Ab before treatment. Tumor growth was measured twice per week ($n = 6$ mice). **c** MC38 tumor-bearing mice (6–8 weeks old female C57BL/6J mice) were treated as (**a**). For cell depletion, mice were injected with 200 μg anti-NK1.1 Ab or 500 μg anti-IFNγ Ab before treatment. Tumor growth was measured twice per week ($n = 6$ mice). **d** MC38 tumor-bearing mice (6–8 weeks old female C57BL/6J mice) i.v. treated with *O*-IMDQ and/or 6 Gy radiation on days 13, 16, and 19. FTY720 was administered at 20 μg one day before treatment initiation and then every other day for 2 weeks. Tumor growth was measured ($n = 6$ mice). **e** *Batf3* knockout mice (6–8 weeks old female) were inoculated with MC38 cells. Mice were treated with *O*-IMDQ and/or 6 Gy radiation on days 10, 13, and 16. Tumor growth was measured ($n = 5$ mice in Ctrl, $n = 6$ mice in the treated group). Data were shown as mean ± SEM and are representative of at least three independent experiments. Statistical analysis was performed using two-way ANOVA. Exact *P* value has been provided in figures; ns not significant. *N* numbers define the biological replicates. Source data are provided as a Source Data file.

observed that early administration of FTY720 abolished the prodrug-induced antitumor effect (Supplementary Fig. 10b). This phenomenon was attributed to the early blockade of T cell entry into tumors, resulting in insufficient T cell presence within the TME to mount an effective therapeutic response. Together, the data suggest that rejuvenation of pre-existing TILs is sufficient for achieving tumor control.

DCs, particularly cDC1s, are pivotal for initiating and sustaining T cell responses[37]. To delineate the contribution of cDC1 to the antitumor effect of TLR7/8 agonist prodrug treatment, we established the MC38 tumor in *Batf3* knockout mice, which lack cDC1s, and treated them with radiotherapy-activated agonist prodrug. As anticipated, the significant antitumoral effect mediated by radiotherapy-activated *O*-IMDQ was markedly diminished in these mice (Fig. 2e). Collectively, these findings underscore that cDC1s and pre-existing CD8⁺ T cells play indispensable roles in radiotherapy-activated *O*-IMDQ therapy.

STING and the MyD88 signaling pathways regulate type I IFN production in response to DC activation

To better understand local activation of DCs, we performed RNA-seq analysis on intratumoral DCs isolated from MC38 tumors treated with radiotherapy-activated *O*-IMDQ, compared to untreated controls. Gene set enrichment analysis (GSEA) revealed significant enrichment in IFNα signaling pathways (Fig. 3a). Moreover, DCs from the treatment group showed elevated expression levels of interferon-stimulated genes (ISGs) involved in DC maturation and antigen presentation, such as *B2m, Stat2, Ifitm1, Ifitm3* and *Mx2*, as well as genes contributing to T cell recruitment, like *Cxcl10* (Fig. 3b). Type I IFN is known to be the key molecule to enhance activation and antigen presentation of DC[38]. Thus, we investigated the necessity of type I IFN signaling in the antitumor efficacy of the agonist prodrug treatment by blocking IFNαR. Administration of anti-IFNαR antibodies resulted in complete loss of the antitumor effect, underscoring the critical role of type I IFN signaling (Fig. 3c). These results suggest that the treatment fosters an intratumoral functional DC-T cell interaction through type I IFN signaling.

TLR7/8 agonists are known to stimulate DC to produce IFN through the MyD88 pathway[39]. Next, we sought to identify which signaling pathways are critical for type I IFN production. Using MyD88 knockout BMDCs, we observed that the upregulation of *IFNα* and *Cxcl10* expression induced by radiotherapy-activated *O*-IMDQ was abolished compared to wild-type (WT) BMDCs, highlighting the essential role of the MyD88 pathway (Fig. 3d, e). However, radiation can induce DC to produce IFN through the cGAS-STING pathway[40]. Thus, we wonder if this pathway is also essential for IFN production. By treating *O*-IMDQ plus radiation in RAW-Lucia ISG WT or STING knockout cells, we discovered an interesting mechanism by which STING signaling also regulates type I IFN production in response to radiotherapy-activated TLR7/8 agonist treatment (Fig. 3f). To further understand the significance of host STING signaling, we inoculated MC38 STING knockout cells into WT C57BL/6 mice, which did not

https://doi.org/10.1038/s41467-025-60769-3

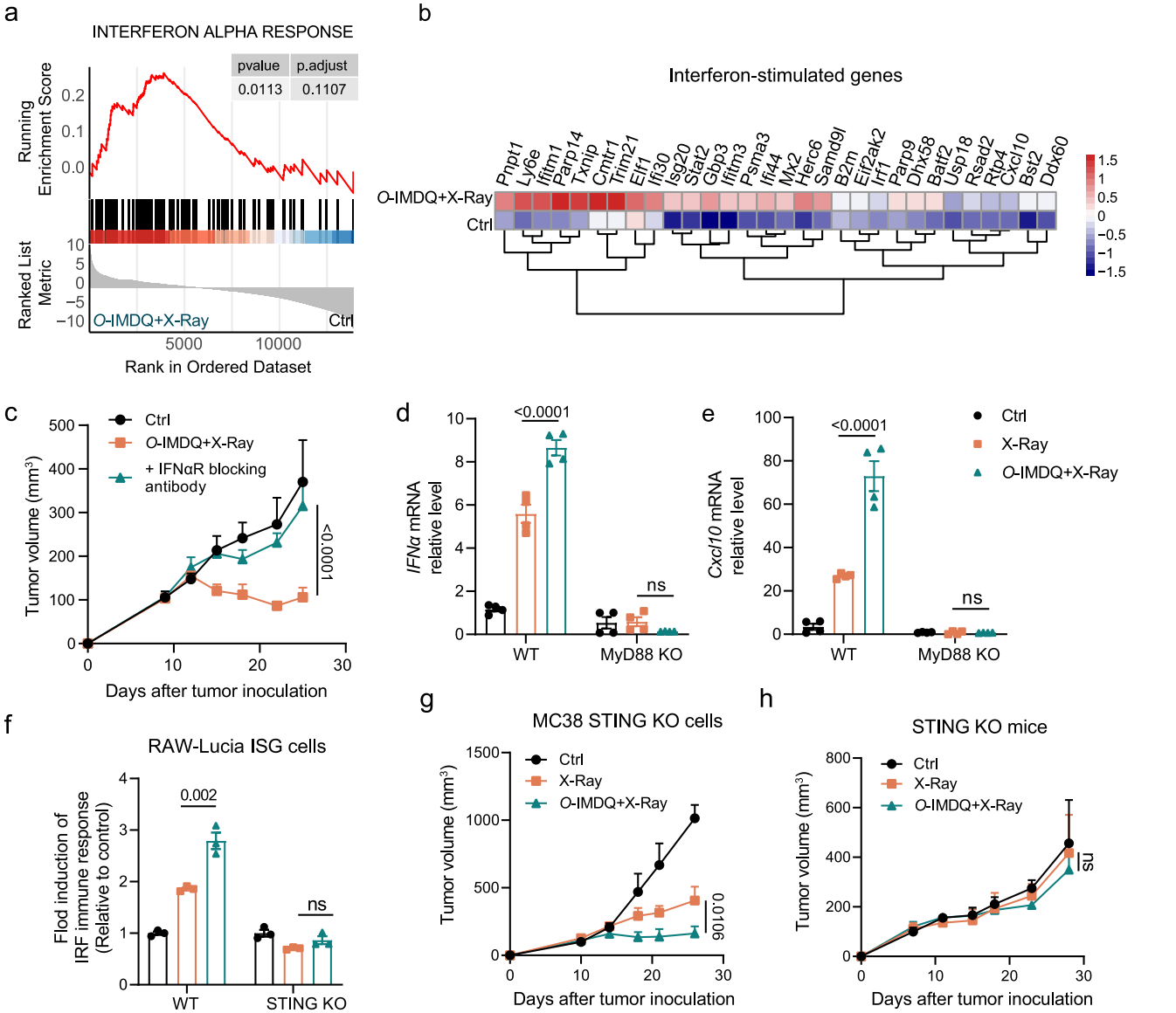

Fig. 3 | STING and MyD88 signalings control type I IFN production responding to TLR7/8 agonist prodrug. a Six to 8 weeks old female C57BL/6J mice ($n = 6$ mice) were inoculated with 5×10^5 MC38 cells. Tumor-bearing mice were treated with PBS or radiotherapy-activated *O*-IMDQ on days 10 and 13 (6 Gy). The mice were sacrificed, and tumor tissues were collected 72 h after the second injection. $CD45^+Ly6C^-MHC\ II^+CD11c^+$ DCs were sorted for RNA-seq. Gene set enrichment analysis of IFNα signaling. **b** Interferon-stimulated genes expression levels were shown. **c** MC38 tumor-bearing mice (6–8 weeks old female C57BL/6J mice) were injected with 500 μg anti-IFNαR Ab before treatment. Tumor growth was measured twice per week ($n = 5$ mice). **d** WT or MyD88 KO BMDCs were stimulated with *O*-IMDQ and/or radiation (20 Gy) for 24 h, *IFNα* mRNA level was analyzed ($n = 4$ cells). **e** WT or MyD88 KO BMDCs were stimulated with *O*-IMDQ and/or radiation (20 Gy) for 24 h, *Cxcl10* mRNA level was analyzed ($n = 4$ cells). **f** RAW-Lucia ISG WT or STING KO cells were stimulated with *O*-IMDQ and/or radiation (20 Gy) for 24 h, ISRE reporter activity was determined ($n = 3$). **g** Six to 8 weeks old female C57BL/6J mice ($n = 5$ mice) were inoculated with 5×10^5 MC38 STING KO cells and i.v. treated with *O*-IMDQ and/or 6 Gy radiation on days 10, 13, and 16. **h** Six to 8 weeks old female STING knockout mice were inoculated with MC38 cells. Mice were i.v. treated with *O*-IMDQ and/or 6 Gy radiation on days 10, 13, and 16. Tumor growth was measured ($n = 5$ mice). Data were shown as mean ± SEM and are representative of at least three independent experiments. Statistical analysis was performed using two-way ANOVA. Exact *P* value has been provided in figures; ns not significant. *N* numbers define the biological replicates. Source data are provided as a Source Data file.

compromise the efficacy of radiotherapy-activated *O*-IMDQ-mediated tumor control, while inoculating MC38 WT tumors with STING knockout C57BL/6 mice diminished its therapeutic efficacy (Fig. 3g, h). These data reveal that the host STING signal is crucial for the treatment effect. Our findings in RAW-Lucia ISG cells also confirm that IMDQ enhanced STING-mediated immune responses (Supplementary Fig. 11). Overall, our findings demonstrate that both STING and MyD88-mediated signaling pathways converge to promote the production of type I IFN, which potently promotes tumor rejection.

TLR7/8 agonist prodrug orchestrates DC-T cells' responses within tumors through type I IFN signal

RNA-seq analysis of intratumoral $CD8^+$ T cells revealed elevated expression levels of genes associated with activation, differentiation, and IFN signaling in the radiotherapy-activated agonist group, indicating the increased T cell responses (Fig. 4a). We further conducted an in-depth investigation into whether and how the DC-T immunity responses within TME is modulated following treatment with TLR7/8 agonist prodrug. Flow cytometry analysis of DCs and $CD8^+$ T cells

https://doi.org/10.1038/s41467-025-60769-3

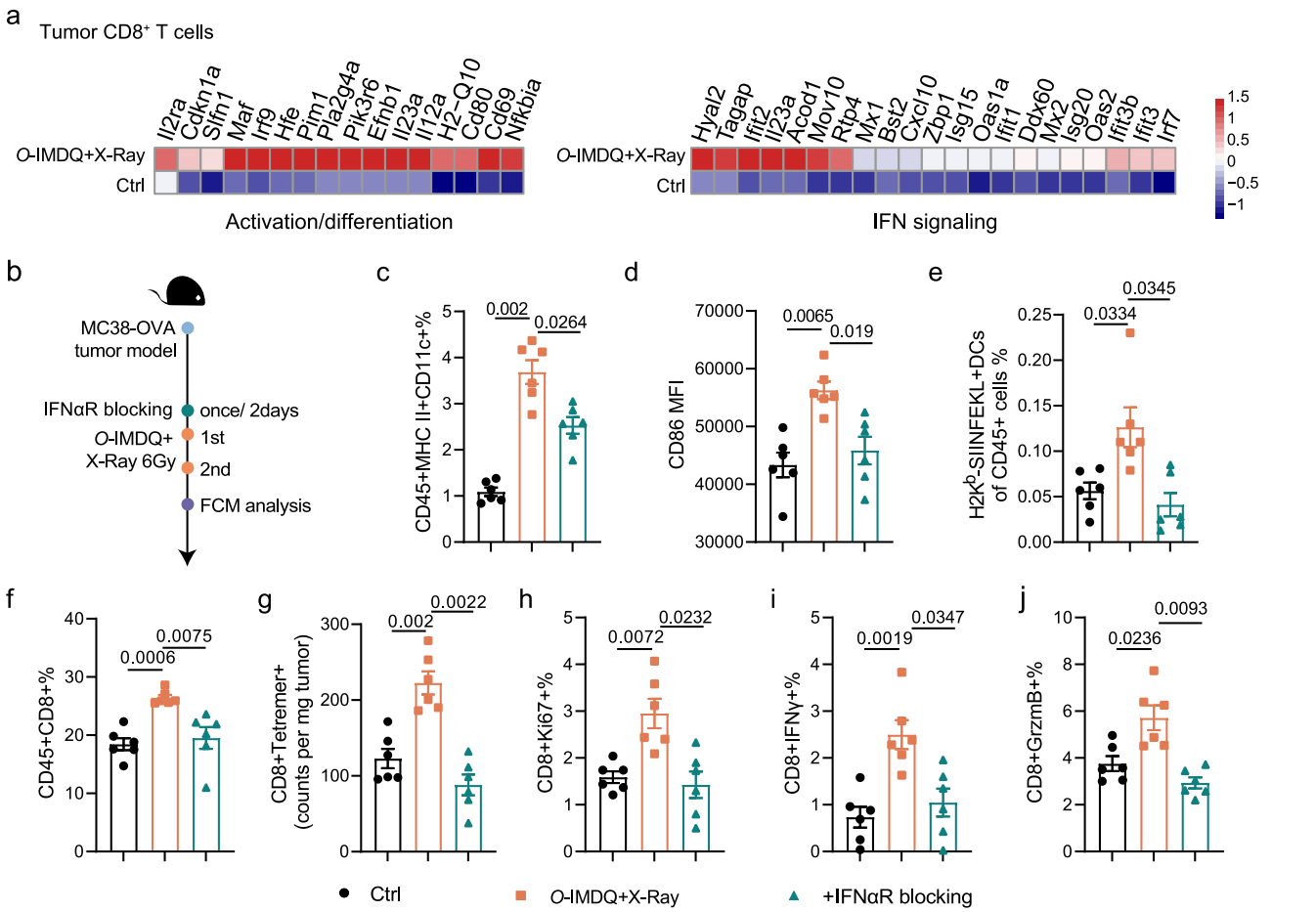

Fig. 4 | TLR7/8 agonist prodrug orchestrates cDC1s to invigorate CD8⁺ T cell responses through type I IFN signal. a Six to 8 weeks old female C57BL/6 mice ($n = 6$ mice) were inoculated with 5×10^5 MC38 cells. Tumor-bearing mice were treated with PBS or radiotherapy-activated *O*-IMDQ on days 10 and 13 (6 Gy). The mice were sacrificed, and tumor tissues were collected 72 h after the second injection. CD45⁺CD3⁺CD8⁺ T cells were sorted for RNA-seq. Gene expression levels were shown. **b** The schematic of radiotherapy-activated TLR7/8 agonist treatment. **c** MC38 tumor-bearing mice (6–8 weeks old female C57BL/6J mice, $n = 6$ mice) were i.v. treated with *O*-IMDQ and/or 6 Gy radiation on days 13 and 16. 500 μg anti-IFNαR Ab was injected before treatment. The mice were sacrificed, and tumor tissues were collected 72 h after the last treatment. CD45⁺MHC II⁺CD11c⁺ DCs were determined by flow cytometry. **d** CD86 expression on DCs was determined by flow cytometry. **e** The antigen presentation function of DCs was determined by flow cytometry. **f** CD45⁺CD8⁺ T cells were determined by flow cytometry. **g** Antigen-specific CD8⁺ T cells were determined by flow cytometry. **h** Ki67 was determined by flow cytometry. **i** IFNγ was determined by flow cytometry. **j** GrzmB was determined by flow cytometry. Data were shown as mean ± SEM and are representative of at least three independent experiments. Statistical analysis was performed using Student's two-tailed unpaired *t*-test. Exact *P* value has been provided in the figures. *N* numbers define the biological replicates. Source data are provided as a Source Data file.

within the tumor was performed at 72 h post-treatment to evaluate immune cell dynamics and functional changes (Fig. 4b). Initially, we observed a rapid increase in the percentage of CD45⁺MHC II⁺CD11c⁺ DCs following radiotherapy-activated *O*-IMDQ treatment (Fig. 4c and Supplementary Fig. 15a). Moreover, the rapid upregulation of the activation marker CD86 on DCs indicated enhanced activation of intratumoral DCs upon TLR7/8 agonist prodrug administration (Fig. 4d). We also observed increasing percentage of the populations of H2K^b-SIINFEKL⁺ DCs, revealing an augmentation in the antigen presentation capacity of DCs within the TME (Fig. 4e). The increasing number, activation and the antigen presentation of DCs following treatment with TLR7/8 agonist prodrug was impaired by using anti-IFNαR antibody to block type I IFN signal (Fig. 4c–e), suggesting that TLR7/8 agonist prodrug treatment could promote intratumoral DC antigen presentation though type I IFN signal.

Next, we investigated how activated DC amplify T cell responses within the TME. Our data demonstrated a significant increase in the percentage of CD8⁺ T cells, particularly antigen-specific T cells, after targeting DCs (Fig. 4f, g and Supplementary Fig. 15b). This finding suggests that TLR7/8 agonist prodrug treatment preferentially activates a subset of CD8⁺ T cells inside the TME, followed by activating DCs, thereby establishing intratumoral DC-T interaction for specific and potent antitumor immunity. In addition, radiotherapy-activated *O*-IMDQ increased Ki67 expression on CD8⁺ T cells, indicating that T cells were expanded inside TME soon after treatment (Fig. 4h). Meanwhile, the percentage of IFNγ⁺ and GrzmB⁺ CD8⁺ T cells was increased, highlighting enhanced cytotoxic activity against tumor cells (Fig. 4i, j and Supplementary Fig. 15b). Importantly, blockade of intratumoral IFNαR rapidly attenuated the T cell responses induced by TLR7/8 agonist prodrug treatment (Fig. 4f–j).

In summary, our findings underscore that radiotherapy-activated *O*-IMDQ orchestrates robust intratumoral DC-T cell immunity responses to shape the TME, promoting tumor rejection in a type I IFN-dependent manner. This mechanistic insight enhances our understanding of how to orchestrate DC-T cell interaction within the TME for enhancing antitumor activity. It also opens a new therapeutic strategy to improve outcomes in cancer immunotherapy.

Optimizing local DC-T cell responses promotes the abscopal effect

Achieving a radiation-induced abscopal effect is an unmet clinical need, suggesting that radiation alone may fail to generate sufficient

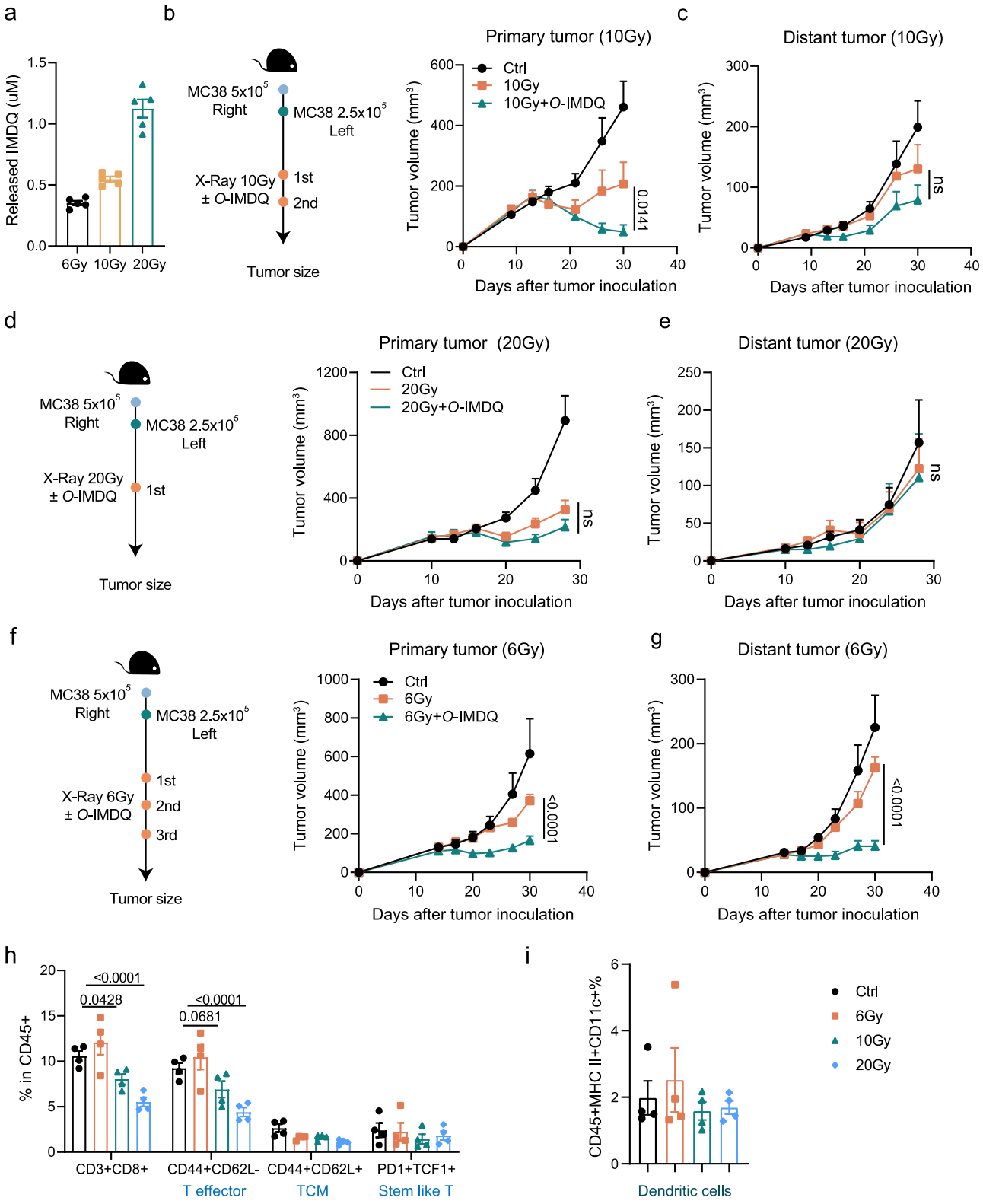

T cells to control distal tumors[41,42]. Our study observed that the amount of IMDQ released in tumors increased in a radiation dose-dependent manner (Fig. 5a). This finding led us to hypothesize that higher doses of radiotherapy combined with the TLR7/8 agonist prodrug could potentially improve both local control of the primary tumors and the abscopal effect on distal tumors. To test this, we employed a bilateral tumor model and different doses of radiation. To maintain the overall radiation dose, we administered either two treatments of 10 Gy (10 Gy × 2) or a single treatment of 20 Gy (20 Gy × 1). Interestingly, treatment with *O*-IMDQ and 10 Gy radiation enhanced suppression of the primary tumor but nearly eliminated the abscopal effect (Fig. 5b, c). Conversely, a single dose of 20 Gy radiation combined with *O*-IMDQ failed to induce tumor rejection compared to radiation alone, indicating a complex relationship between radiation dose and the abscopal effect (Fig. 5d, e). Moreover, we observed only a transient and mild effect on body weight, which rapidly recovered

Fig. 5 | Fractionated low-dose radiotherapy-activated TLR7/8 agonist optimizing local DC-T cell responses promotes abscopal effect. a Concentration of IMDQ released in tumors treated with or without X-ray irradiation (6 Gy, 10 Gy, or 20 Gy) at 1 h after intravenously administrated of *O*-IMDQ, detected by UPLC-MS ($n = 5$ mice). **b** C57BL/6J mice (6–8 weeks old female C57BL/6J mice) were injected subcutaneously with MC38 cells on day 0 and day 2, followed by intravenous administration of *O*-IMDQ and radiotherapy 10 Gy. Tumor volume of irradiated tumors was measured ($n = 6$ mice). **c** Unirradiated tumors were measured ($n = 6$ mice). **d** C57BL/6 J mice (6–8 weeks old female C57BL/6J mice) were injected subcutaneously with MC38 cells on day 0 and day 2, followed by intravenous administration of *O*-IMDQ and radiotherapy 20 Gy. Tumor volume of irradiated tumors was measured ($n = 6$ mice). **e** Unirradiated tumors were measured ($n = 6$ mice). **f** C57BL/6J mice (6–8 weeks old female C57BL/6J mice) were injected subcutaneously with MC38 cells on day 0 and day 2, followed by intravenous administration of *O*-IMDQ and radiotherapy 6 Gy. Tumor volume of irradiated tumors was measured ($n = 6$ mice in Ctr and X-Ray, $n = 7$ mice for X-Ray+*O*-IMDQ). **g** Unirradiated tumors were measured ($n = 6$ mice in Ctr and X-Ray, $n = 7$ mice for X-Ray+*O*-IMDQ). **h** MC38 tumor-bearing mice (6–8 weeks old female C57BL/6J mice) were treated by different dose radiation. Seventy-two hours after the last treatment, $CD8^+$ T cells were determined by flow cytometry ($n = 4$ mice). **i** MC38 tumor-bearing mice (6–8 weeks old female C57BL/6J mice) were treated by different dose radiation. Seventy-two hours after the last treatment, DCs was determined by flow cytometry ($n = 4$ mice). Data were represented as means ± SEM and are representative of at least two independent experiments. Statistical analysis was performed using Student's two-tailed unpaired *t*-test (**h**, **i**) or two-way ANOVA (**b**–**g**). Exact *P* value has been provided in figures; ns, not significant. *N* numbers define the biological replicates. Source data are provided as a Source Data file.

thereafter (Supplementary Fig. 12d). Then, we hypothesize that lower radiation doses may preserve T cell function better, potentially enhancing the abscopal effect through synergistic TLR signaling. Indeed, we observed that three treatments of 6 Gy (6 Gy × 3) alone fails to control both local and distal tumor, but combing a TLR7/8 agonist prodrug-induced local tumor control and potentiated the abscopal effect (Fig. 5f, g). Furthermore, we explored lower radiation doses (e.g., 4 Gy × 3) and found that combining 4 Gy radiation with the same dose of *O*-IMDQ failed to control tumor growth, since lower radiation doses might not release sufficient IMDQ (Supplementary Fig. 12a). However, increasing the dose of *O*-IMDQ with 4 Gy radiation could promote impressive control of both local and distal tumors (Supplementary Fig. 12b, c). In summary, neither high nor low dose radiation alone triggered the abscopal effect. Combining fractionated, low-dose radiotherapy with *O*-IMDQ could induce a remarkable abscopal effect, while combining high-dose radiotherapy diminished the abscopal effect. These findings open new avenues for developing strategies that balance radiation and drug doses to mediate synergistic effects for both local and distal tumor control.

Our data also revealed that pre-existing T cells within the tumor were adequate for local tumor control (Fig. 2d). However, it remains unclear whether irradiated intratumoral T cells are essential for the abscopal effect on distal tumors. Measurement of T cells and DCs in tumors treated with FTY720 and varying doses of radiation showed a decrease in T effector cells with increasing radiation dose (Fig. 5h and Supplementary Fig. 15c), while the number of DCs remained unaffected (Fig. 5i). This suggests that the ability of DCs to prime T cells from DLN remains intact. Thus, the presence of viable T cells by low dose (4–6 Gy) within the tumor appears crucial for mediating the abscopal effect. In summary, our results indicate that the successful combination of radiotherapy and TLR7/8 agonist prodrug to promote abscopal effect depends significantly on optimizing the doses of radiation and prodrug dose to enhance local DC-T cell responses.

Local immune activation by radiotherapy-activated *O*-IMDQ decreases cold tumor metastasis

Tumor metastasis is a major contributor to treatment failure and poses life-threatening risks for cancer patients[43]. It has been difficult to define whether local immunity is required for controlling metastasis. The radiation-sensitive prodrug opens a new tool to address this question. We employed dual cold tumor models to evaluate the therapeutic efficacy of radiotherapy-activated *O*-IMDQ against both localized and metastatic tumors. Firstly, poor immunogenic B16/F10 tumor cells were subcutaneously inoculated and subsequently intravenously injected one day before treatment to establish tumor models mimicking local and metastatic tumors. We found that treatment with radiotherapy-activated *O*-IMDQ not only effectively controlled local tumor growth but also significantly reduced lung metastasis, as evidenced by decreased colony formation (Fig. 6a–c). Furthermore, we investigated the treatment's impact on spontaneous metastasis using the 4T1 mammary carcinoma model, known for its poor immunogenicity, few TILs and spontaneous metastasis within ten days post-implantation. Mice bearing established 4T1 tumors were treated with radiotherapy-activated *O*-IMDQ, followed by assessment of lung metastasis using IVIS imaging. The results demonstrated a marked reduction in lung metastasis and prolonged survival compared to radiation alone (Fig. 6d–f). These findings underscore the therapeutic potential of radiotherapy-activated *O*-IMDQ in suppressing metastatic spread and improving overall survival outcomes. To further evaluate the translational potential of our prodrug, we constructed a humanized $CD34^+$ mice model. The result was consistent with our findings in mouse tumor models, showing reduced tumor growth upon prodrug treatment (Supplementary Fig. 14).

In conclusion, our study provides compelling evidence that local immunity is required for controlling metastasis. This approach holds promise for clinical application in combating tumor metastasis and enhancing patient prognosis in cancer treatment.

Discussion

Understanding the pivotal role of intratumoral DC-T cell responses in cancer immunotherapy has been challenging[7]. Recent research has increasingly highlighted the significance of these responses within the TME[44]. Traditionally, immune activation against tumors was thought to primarily occur in DLNs[4,45]. However, it is not easy to define the contribution of immune activity that occurs within the TME itself. We propose that the quality and extent of crosstalk between intratumoral DCs and T cells could determine the success or failure of antitumor immune responses within the TME[46]. To limit the primary activation of DC-T cells inside TME, we have explored a technique to modify the TLR7/8 agonist IMDQ with a single oxygen atom, rendering it inactive until precisely reactivated by local radiotherapy within the TME. While previous studies have explored the use of radiotherapy to activate prodrugs, their approaches have been primarily limited to chemotherapy or have focused on different chemical modifications[27,31]. For example, some strategies have employed sulfonyl azide and phenyl azide caging groups to achieve radiation-triggered drug release[27], while others have primarily focused on N-oxide modifications in anticancer prodrugs, such as camptothecin (CPT), to enhance direct tumor cytotoxicity[31]. Building upon this foundation, our collaborative research takes a distinct approach by leveraging radiotherapy-induced reduction to achieve immune-specific intratumoral activation of a TLR7/8 agonist prodrug (*O*-R848)[47]. Although the chemical basis for N-oxide reduction by radiotherapy is well established, its immunological implications remain largely unexplored. Furthermore, the essential role of DC-T cell interaction within TME for local and distal immunity has been difficult to address. Here, we demonstrate that TLR7/8 activation within the TME not only enhances local tumor control but also induces abscopal effects through type I IFN signaling, providing new insights into the regulation of DC-T cell interactions and their role in systemic antitumor immunity. Importantly, though TLR7/8

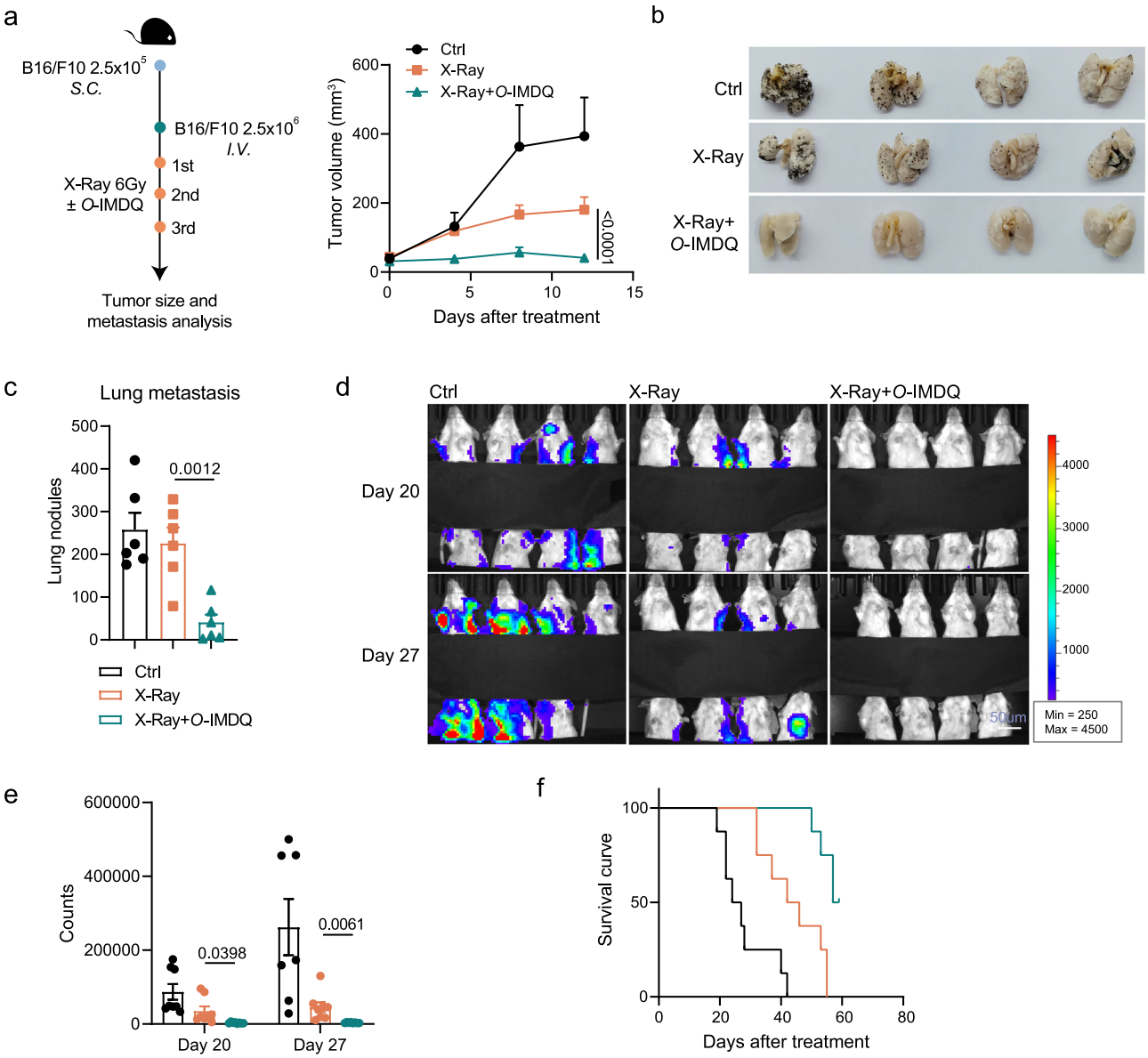

Fig. 6 | Local immunity activation by radiotherapy-activated *O*-IMDQ decreases cold tumor metastasis. a Six to 8 weeks old female C57BL/6J mice ($n = 6$ mice) were inoculated with 2.5×10^5 B16F10 cells. After 1 week, 2.5×10^6 B16/F10 cells were intravenously injected. Tumor-bearing mice were i.v. treated with *O*-IMDQ and/or 6 Gy radiation on days 8, 11, and 14. The local tumor volume was measured. **b** The photos of lung metastasis. **c** The colony number on the lung was counted. **d** Six to 8 weeks old Balb/c mice ($n = 8$ mice) were inoculated with 2×10^5 4T1-luc2 cells. Tumor-bearing mice were i.v. treated with *O*-IMDQ and/or 6 Gy radiation on days 10, 13, and 17. The metastasis of the lung was measured by the IVIS Spectrum. Scale bar = 50 um. **e** The counts on the lung was counted ($n = 8$ mice). **f** Survival curve was shown. Data were represented as means ± SEM and are representative of at least two independent experiments. Statistical analysis was performed using Student's two-tailed unpaired *t*-test (**c**) or two-way ANOVA (**a**, **e**). Exact *P* value has been provided in figures. *N* numbers define the biological replicates. Source data are provided as a Source Data file.

agonist activates macrophages[35], depletion of macrophages using CSF1R antibody did not affect therapy response. A high dose of radiation could activate more DCs to DLN. But diminished distal immunity suggests the essential role of DC-TILs for distal protection. These results suggest that DCs are the primary antigen-presenting cell (APC) in this context.

Mechanically, this prodrug stimulates robust production of type I IFNs via both the STING and MyD88 signaling pathways, which are crucial for augmenting DC-mediated T cell responses against tumors[39,40]. Type I IFNs orchestrate a multifaceted antitumor response, including direct cytotoxic effects on tumor cells, enhancement of antigen presentation, activation of immune cells, and modulation of the TME[38,48]. In our study, blockade of IFNαR not only attenuated the intratumoral DC-T immunity responses but also abolished the therapeutic effect. While IMDQ activates the MyD88 signaling pathway[49], radiotherapy mainly triggers the STING pathway[40,50]. The data suggest that there might be a positive loop for the STING and MyD88 pathway after radiation-activated TLR7/8. Consistently, recent studies have suggested that TLR-induced NF-κB activation can enhance STING signaling by altering microtubule-mediated STING trafficking[51], which is consistent with our findings. But another study shows that MyD88 and STING may form a complex to drive downstream immunity responses[52], so the detailed mechanism in our specific context warrants further exploration.

During antitumor immune responses, T cells can originate from two major sources: pre-existing TILs and newly activated T cells migrating from DLN to the tumor site[53]. Early administration of FTY720 abolished the prodrug-induced antitumor effect. Conversely, when

FTY720 was administered just before prodrug therapy initiation, thereby only preventing further T cell infiltration into tumors, pre-existing TILs were adequate for controlling tumors treated with targeted radiation-activated prodrug. This finding suggests that enhanced DC-T cell responses within the TME sufficiently control local tumors.

Achieving local control and the abscopal effect through advanced local radiation has been a longstanding unmet clinical need[54]. However, demonstrating an abscopal effect with either low or high doses of radiation remains challenging[16,55]. High doses can effectively control local tumors but impair TILs for abscopal effect, while low doses often fail to reactivate DC-T cell immunity, even fail to control local tumors, likely limiting their potential to induce an abscopal effect[42]. Recent studies using tumor-specific photoconversion have demonstrated that radiation therapy results in a loss of $CD8^+$ T cell recirculation from the tumor to the DLN and distal untreated tumors shortly after radiation[56]. These findings underscore the pivotal role of pre-existing TILs in both local tumor control and distal tumor rejection and support the importance of optimizing DC-T cell responses within the TME for achieving these effects. In our study, we observed that high-dose radiation reduces T cell numbers and loses the abscopal effect. To explore if low doses of radiation might synergize with local activation of TLRs to have a strong abscopal effect, we have explored and defined a fractionated, low-dose radiotherapy (6 Gy × 3 or 4 Gy × 3) which can effectively activate TLR7/8 agonist-mediated immune responses within tumors, leading to better primary and distal tumor control. Clinically, conventional radiation (RT) typically employs lower doses per fraction (1.8–2.0 Gy) over more than 30 sessions, ensuring cumulative tumor control while minimizing normal tissue toxicity. In contrast, stereotactic body radiotherapy (SBRT) delivers higher doses per fraction (typically 8–20 Gy) over fewer sessions (3–5 fractions), allowing for precise tumor targeting while limiting collateral damage[57]. Our strategy of 4-6 Gy × 3 fractions lies between these two clinical approaches, striking a balance between dose intensity and precision. This intermediate dosing regimen holds potential for clinical translation, particularly in enhancing abscopal effects for distal tumor control. Therefore, our study not only provides a mechanistic understanding of radiation-enhanced immune activation but also paves the way for optimizing radiation dose and fractionation strategies in clinical settings to maximize therapeutic efficacy. Humanized $CD34^+$ mice model further evaluates the translational potential of our prodrug. However, the number of human immune cells and tumor-specific T cells are limited. We acknowledge the clinical challenges that remain, particularly in optimizing delivery and radiotherapy dosing and timing in humans. Further, we will explore combination therapies, such as an mRNA vaccine or checkpoint inhibitors.

In conclusion, our research highlights the importance of intratumoral immune responses for tumor control through the use of radiotherapy-activated TLR7/8 agonists, and investigates if and how these agonists optimize DC-T cell interactions within the TME to effectively control both local and distal tumors. Optimizing local DC-T cell responses by TLR7/8 agonist prodrug treatment modulates the TME, making cold tumors susceptible to immunotherapy and reducing metastasis. Understanding these intratumoral immune interactions holds promise for enhancing immunotherapeutic strategies aimed at improving tumor control and patient outcomes.

Methods

Mice

C57BL/6J female mice (#213) and Babl/c mice (#211) were purchased from Beijing Vital River Laboratory Animal Technology Co., Ltd (Considering that female mice exhibit lower aggression, which makes them more suitable for group breeding with reduced management difficulty). Batf3 knockout mice and STING knockout mice were purchased from The Jackson Laboratory. MyD88 knockout mice were kindly provided by Dr. Xiaoyu Hu's Lab (School of Medicine, Tsinghua University). All mice were maintained under specific pathogen–free conditions. All animal care and experimental procedures were approved by the Animal Care and Use Committees (IACUC) of Tsinghua University. The experimental and control animals were co-housed. In none of the experiments did the size of the tumor graft surpass 2 cm in any two dimensions (according to the limits defined by the IACUC protocol). For euthanasia, the mice were euthanized by carbon dioxide according to the approved protocols.

Cell lines and reagents

MC38 was purchased from Cytion (#305223). B16/F10 was purchased from the American Type Culture Collection (#CR6475). MC38-OVA was selected from a signal-cell clone after transfection by lentivirus-expressed OVA[58]. 4T1-luc2 was kindly provided by Dr. Wei Liang's Lab (Institute of Biophysics, Chinese Academy of Sciences) and cultured in RPMI-1640 supplemented with 10% FBS and 1% penicillin-streptomycin. RAW-Lucia ISG cells (#rawl-isg), RAW-Lucia ISG-KO-STING cells (#rawl-kostg) and Human TLR8 reporter HEK293 cells (#hkb-htlr8) were purchased from InvivoGen. RAW-Blue reporter cells were kindly provided by Dr. Zhibo Liu's Lab. All cells, 4T1-luc2 excepted, were cultured in DMEM supplemented with 10% FBS and 1% penicillin-streptomycin. The cell lines from manufacturers were not authenticated. The MC38-OVA was authenticated by flow cytometry.

QUANTI-Blue solution and QUANTI-Luc 4 Lucia/Gaussia were purchased from Invivogen. FTY720 was purchased from Sigma Aldrich. Anti-CD4 (GK1.5, Bioxcell #BE0003-1), anti-NK1.1 (PK136, Bioxcell #BE0036), anti-CD8 (53-5.8, Bioxcell #BE0004-1), anti-CSF1R (AFS98, Bioxcell #BE0213), IFNγ neutralization antibody (XMG1.2, #BE0055), and IFNαR blocking antibody (MAR1-5A3, #BE0241) were purchased from BioXCell. Recombinant murine GM-CSF (#315-03-20UG) were purchased from PeproTech.

IMDQ was purchased from WuXi AppTec in a customized manner and used as received. Chloroform ($CHCl_3$, #167735000), dichloromethane (DCM, #BD00959791), ethyl acetate (EtOAc, #937345), anhydrous Na_2SO_4 (#BD31900), $Na_2S_2O_3$ (#955588), $NaHCO_3$ (#BD151377), di-tert-butyl dicarbonate (Boc_2O, #BD32840), meta-Chloroperoxybenzoic acid (m-CPBA, #A84043) were purchased from Innochem, J&K Scientific, Bidepharm, and used as received.

Chemical synthesis method of *O*-IMDQ

To a solution of parent drug IMDQ (0.5 g, 1.6 mmol, 1.0 eq.) in 10 mL $CHCl_3$ was added a solution of Boc_2O (0.065 g, 0.3 mmol, 0.2 eq.) in 5 mL of $CHCl_3$ overnight. Then the solution was diluted with DCM and washed with sat. $NaHCO_3$ aqueous solution. The organic layer was dried over anhydrous Na_2SO_4 to give an intermediate 1 (260.0 mg). To a mixture of intermediate 1 (250.0 mg, 0.6 mmol, 1.0 eq.) in 3 mL DCM was added *m*-CPBA (123.4 mg, 0.6 mmol, 85% purity, 1.0 eq.) at 0 °C and stirred at 0 °C for 0.5 h. Then the mixture was quenched by sat. $Na_2S_2O_3$ aqueous solution (5 mL), extracted with EtOAc (20 mL × 3). The combined organic layers were washed with 30 mL of sat. $NaHCO_3$ aqueous solution, dried over anhydrous Na_2SO_4, and concentrated under reduced pressure to give an intermediate 2 (88.0 mg, crude). Then a mixture of intermediate 2 (75.0 mg, 175.3 µmol, 1.0 eq.) in EtOAc/HCl (1 mL) was stirred at 25 °C for 0.5 h. The reaction mixture was purified by prep-HPLC to give *O*-IMDQ (40.3% yield) as a yellow solid.

Molecular docking and kinetic simulation

Informatics analyses of the PDB bind datasets were done using RDKit and Biopython. Molecular modeling tasks were performed using various modules in Schrödinger Suites 2018-1 (Schrödinger, LLC, NY). Co-crystal structure of the activated state of human TLR8 dimers with an imidazolequinoline agonist (PDB ID: 3W3L) was retrieved from RCSB Protein Data Bank, and was then prepared and minimized using

Protein Preparation Wizard. IMDQ, as well as its N-oxide *O*-IMDQ, was subsequently docked into the agonist binding site using Glide. The docked ternary structures of TLR8 dimer-IMDQ and TLR8 dimer-*O*-IMDQ were then solvated and neutralized. Molecular dynamics simulations were performed in Desmond. Each of the initial models was first relaxed using a six-step default protocol, and was then subjected to a 30 ns NPT simulation with temperature fixed at 300 K and pressure at 1.01 bar. After each simulation was completed, RMSD fluctuations and protein–ligand interactions could be calculated in the Simulation Interaction Diagram module based on the resulting trajectories. For protein-ligand complexes, MM-GBSA calculations were performed in Prime, where the VSGB solvation model was selected and residues within 3 Å from the ligand were treated as flexible.

Radiation strategy

Irradiator: X-ray generator (RS2000 Pro 225, 225 kV, 17.7 mA, Rad Source Technologies, Inc.). For cellular studies, live cells were degassed and irradiated with a total dose of 10–20 Gy at a dose rate of 2.87 Gy/min. For in vivo studies, local irradiation of implanted tumors was performed using a customized mouse jig. Tumors were selectively irradiated with a total dose of 6–20 Gy at a dose rate of 2.87 Gy/min, while the rest of the body was shielded using 5-mm-thick lead plates.

Reporter cell line assays

RAW-Blue reporter cells, RAW-Lucia ISG cells, RAW-Lucia ISG-KO-STING cells, and Human TLR8 reporter HEK293 cells were plated in a 96-well plate at a density of 5×10^4 cells/well. The cells were treated with agonist prodrugs plus radiation 10 Gy for 24 h. The supernatant was tested with QUANTI-Blue and Luciferase Reporter System.

BMDCs generation and activation

BMDCs were generated by culturing bone marrow cells in the presence of rmGM-CSF (20 ng/ml, #315-03-20UG) for 6 days. Then the BMDCs were treated with IMDQ alone, *O*-IMDQ alone, and *O*-IMDQ + X-ray (10 Gy). After 24 h incubation, cells were sorted, and surface markers CD80/86 and antigen presentation were analyzed on flow cytometry (BD Bioscience). Supernatant was collected and measured by BD Cytometric Bead Array (CBA) Mouse Inflammation Kit (BD, #552364).

Gene expression analysis using quantitative PCR

WT or MyD88 KO BMDCs were stimulated with *O*-IMDQ and/or radiation for 24 h. Total mRNA was isolated from cells using Trizol (Takara, #9109) following the manufacturer's instructions. Reverse transcription was performed on 1 mg total mRNA per sample using PrimeScript RT Reagent Kit with gDNA Eraser (Takara, #RR047Q) according to the manufacturer's instructions. For the qRT-PCR analysis, SYBR Green Supermix (BioRad, #1708880) was used according to the manufacturer's instructions. qPCR primers were listed: *IFNα* Fwd-TCCATCAGCAGCTCAATGACC; Rev-GCTGTGTTTCTTCTCTCTCAGG; *Cxcl10* Fwd-GAGTGGGACTCAAGGGATC; Rev-TTCTTTTTCATCGTGG CAATGATCTC.

Transcriptomic analysis and gene set enrichment analysis

DCs and TILs were isolated from MC38 tumor-bearing mice 72 h after the second treatment. Total RNA extraction, mRNA library construction, and sequencing were established by BGI. The clean reads were mapped to the genome using HISAT2 (v2.0.4). The expression level of a gene was calculated by RSEM (v1.2.12). The RNA-Seq raw data were processed through the standard RNA-Seq analysis pipeline. Differential-expression analysis was carried out with DESeq2 version 1.24.0 (http://bioconductor.org/about/removed-packages/) in R v.3.3.1 (http://cran.r-project.org/). Genes were considered to be differentially expressed if the adjusted *P* was less than 0.05. The identified gene set involved in a specific pathway was further analyzed with GSEA.

Flow cytometry analysis

Tumor tissues were isolated from sacrificed mice, minced into small pieces and digested for 1 h at 37 °C with 300 U/ml type 1 A Collagenase (Gibco, #17018029) and 0.1 mg/ml DNase (Sigma, #9003-98-9). Digested tissues were filtered through a 70-mm nylon cell strainer (Falcon, #352350). The single cell suspensions were incubated with specific antibodies for 30 min. Dead cells were stained with Fixable Viability Dye (eBioscience, #65-0866-14). For intracellular cytokine staining, cells were fixed and permeabilized using the FoxP3/Transcription Factor Staining Buffer Set (eBioscience, #00-5523-00) for transcription factors according to the manufacturer's instructions. Samples were analyzed on a flow cytometer (BD Bioscience). Data analysis was performed using FlowJo software (TreeStar).

Tumor growth and treatment

About 5×10^5 MC38 cells and 2.5×10^5 B16/F10 cells were subcutaneously injected into the right flank of 6–8- week-old female C57BL/6J mice. About 2×10^5 4T1-luc2 were injected into the mammary fat pad of 6–8 weeks old female Babl/c mice. Tumor-bearing mice were randomly grouped into treatment groups when tumors grew to around 80–100 mm^3. For radiotherapy-activated prodrug treatment, three doses of 50 μg/mice prodrug (*O*-IMDQ, *O*-R848 or *O*-BBIQ) were intravenously given with a 3-day interval, then preformed radiation 1 h later. For CSF1R, NK1.1, $CD4^+$ T cell and $CD8^+$ T cell depletion, 200 μg antibodies were intraperitoneally injected 1 day before treatment initiation and then twice a week for 2 weeks. For IFNγ and IFNαR blockade, 500 μg neutralization antibodies were intratumorally injected 1 day before treatment initiation and then twice a week for 2 weeks. For FTY720 (Sigma, #162359-56-0) treatment, 20 μg FTY720 was intraperitoneally administered in different tumor stages and then every other day for 2 weeks. For the abscopal model, C57BL/6J mice were injected subcutaneously with MC38 cells on day 0 and day 2, followed by intravenous administration of *O*-IMDQ and radiotherapy. For the metastasis model, C57BL/6J mice were inoculated with 2.5×10^5 B16F10 cells. After 1 week, 2.5×10^6 B16F10 cells were intravenously injected. Tumor-bearing mice were i.v. treated with *O*-IMDQ and/or radiation on days 8, 11, and 14. Tumor volumes were measured twice a week and calculated by length × width × height/2. All results were repeated at least three times independently with similar results.

Statistical analysis

All data analyses were performed with GraphPad Prism statistical software (v8.0) and shown as mean ± SEM. Student's two-tailed unpaired *t*-test or one/two-way ANOVA analysis was used to calculate statistical significance for the difference in a particular measurement between groups. *N* numbers define the biological replicates.

Reporting summary

Further information on research design is available in the Nature Portfolio Reporting Summary linked to this article.

Data availability

All data are included in the Supplementary Information or available from the authors, as are unique reagents used in this Article. The raw numbers for charts and graphs are available in the Source Data file whenever possible. The RNA-seq data have been deposited in Gene Expression Omnibus (accession no. GSE276255) under the https://www.ncbi.nlm.nih.gov/geo/query/acc.cgi?acc=GSE276255. Source data are provided with this paper.

References

1. Palucka, K. & Banchereau, J. Cancer immunotherapy via dendritic cells. *Nat. Rev. Cancer* **12**, 265–277 (2012).

2. Heras-Murillo, I., Adan-Barrientos, I., Galan, M., Wculek, S. K. & Sancho, D. Dendritic cells as orchestrators of anticancer immunity and immunotherapy. *Nat. Rev. Clin. Oncol.* **21**, 257–277 (2024).
3. Wculek, S. K. et al. Dendritic cells in cancer immunology and immunotherapy. *Nat. Rev. Immunol.* **20**, 7–24 (2020).
4. Roberts, E. W. et al. Critical role for CD103(+)/CD141(+) dendritic cells bearing CCR7 for tumor antigen trafficking and priming of T cell immunity in melanoma. *Cancer Cell* **30**, 324–336 (2016).
5. Garris, C. S. et al. Successful anti-PD-1 cancer immunotherapy requires T cell-dendritic cell crosstalk involving the cytokines IFN-gamma and IL-12. *Immunity* **55**, 1749 (2022).
6. Spranger, S., Dai, D., Horton, B. & Gajewski, T. F. Tumor-residing Batf3 dendritic cells are required for effector T cell trafficking and adoptive T cell therapy. *Cancer Cell* **31**, 711–723.e714 (2017).
7. Broz, M. L. et al. Dissecting the tumor myeloid compartment reveals rare activating antigen-presenting cells critical for T cell immunity. *Cancer Cell* **26**, 938 (2014).
8. Maier, B. et al. A conserved dendritic-cell regulatory program limits antitumour immunity. *Nature* **580**, 257–262 (2020).
9. McLaughlin, M. et al. Inflammatory microenvironment remodelling by tumour cells after radiotherapy. *Nat. Rev. Cancer* **20**, 203–217 (2020).
10. Rodriguez-Ruiz, M. E. et al. Abscopal effects of radiotherapy are enhanced by combined immunostimulatory mAbs and are dependent on CD8 T cells and crosspriming. *Cancer Res.* **76**, 5994–6005 (2016).
11. Rodriguez-Ruiz, M. E., Vitale, I., Harrington, K. J., Melero, I. & Galluzzi, L. Immunological impact of cell death signaling driven by radiation on the tumor microenvironment. *Nat. Immunol.* **21**, 120–134 (2020).
12. Watanabe, T., Sato, G. E., Yoshimura, M., Suzuki, M. & Mizowaki, T. The mutual relationship between the host immune system and radiotherapy: stimulating the action of immune cells by irradiation. *Int. J. Clin. Oncol.* **28**, 201–208 (2023).
13. Cytlak, U. M. et al. Immunomodulation by radiotherapy in tumour control and normal tissue toxicity. *Nat. Rev. Immunol.* **22**, 124–138 (2022).
14. Golden, E. B. et al. Radiation fosters dose-dependent and chemotherapy-induced immunogenic cell death. *Oncoimmunology* **3**, e28518 (2014).
15. Yin, L. et al. Effect of low-dose radiation therapy on abscopal responses to hypofractionated radiation therapy and anti-PD1 in mice and patients with non-small cell lung cancer. *Int. J. Radiat. Oncol. Biol. Phys.* **108**, 212–224 (2020).
16. Menon, H. et al. Influence of low-dose radiation on abscopal responses in patients receiving high-dose radiation and immunotherapy. *J. Immunother. Cancer* **7**, 237 (2019).
17. Demaria, S. & Formenti, S. C. The abscopal effect 67 years later: from a side story to center stage. *Br. J. Radio.* **93**, 20200042 (2020).
18. Lai, J. Z. et al. Abscopal effects of local radiotherapy are dependent on tumor immunogenicity. *Front. Oncol.* **11**, 690188 (2021).
19. Galluzzi, L., Aryankalayil, M. J., Coleman, C. N. & Formenti, S. C. Emerging evidence for adapting radiotherapy to immunotherapy. *Nat. Rev. Clin. Oncol.* **20**, 543–557 (2023).
20. Sun, H. et al. Targeting toll-like receptor 7/8 for immunotherapy: recent advances and prospectives. *Biomark. Res.* **10**, 89 (2022).
21. Ackerman, S. E. et al. Immune-stimulating antibody conjugates elicit robust myeloid activation and durable antitumor immunity. *Nat. Cancer* **2**, 18–33 (2021).
22. Varshney, D., Qiu, S. Y., Graf, T. P. & McHugh, K. J. Employing drug delivery strategies to overcome challenges using TLR7/8 agonists for cancer immunotherapy. *AAPS J.* **23**, 90 (2021).
23. Mullins, S. R. et al. Intratumoral immunotherapy with TLR7/8 agonist MEDI9197 modulates the tumor microenvironment leading to enhanced activity when combined with other immunotherapies. *J. Immunother. Cancer* **7**, 244 (2019).
24. Zuniga, L. A. et al. Intratumoral delivery of TransCon() TLR7/8 agonist promotes sustained anti-tumor activity and local immune cell activation while minimizing systemic cytokine induction. *Cancer Cell Int.* **22**, 286 (2022).
25. Melero, I., Castanon, E., Alvarez, M., Champiat, S. & Marabelle, A. Intratumoural administration and tumour tissue targeting of cancer immunotherapies. *Nat. Rev. Clin. Oncol.* **18**, 558–576 (2021).
26. Ghosn, M. et al. Intratumoral immunotherapy: is it ready for prime time?. *Curr. Oncol. Rep.* **25**, 857–867 (2023).
27. Geng, J. et al. Switching on prodrugs using radiotherapy. *Nat. Chem.* **13**, 805–810 (2021).
28. Li, X., Sun, H., Lu, Y. & Xing, L. Radiotherapy-triggered prodrug activation: a new era in precise chemotherapy. *Med* **3**, 600–602 (2022).
29. Fu, Q. et al. Radiotherapy activates picolinium prodrugs in tumours. *Nat. Chem.* **16**, 1348–1356 (2024).
30. Fu, Q. et al. External-radiation-induced local hydroxylation enables remote release of functional molecules in tumors. *Angew. Chem. Int. Ed. Engl.* **59**, 21546–21552 (2020).
31. Ding, Z. et al. Radiotherapy reduces N-oxides for prodrug activation in tumors. *J. Am. Chem. Soc.* **144**, 9458–9464 (2022).
32. Farrer, N. J., Higgins, G. S. & Kunkler, I. H. Radiation-induced prodrug activation: extending combined modality therapy for some solid tumours. *Br. J. Cancer* **126**, 1241–1243 (2022).
33. Tanji, H., Ohto, U., Shibata, T., Miyake, K. & Shimizu, T. Structural reorganization of the Toll-like receptor 8 dimer induced by agonistic ligands. *Science* **339**, 1426–1429 (2013).
34. Loh, Z. H. et al. Observation of the fastest chemical processes in the radiolysis of water. *Science* **367**, 179–182 (2020).
35. Rodell, C. B. et al. TLR7/8-agonist-loaded nanoparticles promote the polarization of tumour-associated macrophages to enhance cancer immunotherapy. *Nat. Biomed. Eng.* **2**, 578–588 (2018).
36. Premenko-Lanier, M., Moseley, N. B., Pruett, S. T., Romagnoli, P. A. & Altman, J. D. Transient FTY720 treatment promotes immune-mediated clearance of a chronic viral infection. *Nature* **454**, 894–898 (2008).
37. Hildner, K. et al. Batf3 deficiency reveals a critical role for CD8alpha + dendritic cells in cytotoxic T cell immunity. *Science* **322**, 1097–1100 (2008).
38. Liang, Y., Hannan, R. & Fu, Y. X. Type I IFN activating type I dendritic cells for antitumor immunity. *Clin. Cancer Res.* **27**, 3818–3824 (2021).
39. Fisch, D. et al. Molecular definition of the endogenous Toll-like receptor signalling pathways. *Nature* **631**, 635–644 (2024).
40. Deng, L. et al. STING-dependent cytosolic DNA sensing promotes radiation-induced type I interferon-dependent antitumor immunity in immunogenic tumors. *Immunity* **41**, 843–852 (2014).
41. Ngwa, W. et al. Using immunotherapy to boost the abscopal effect. *Nat. Rev. Cancer* **18**, 313–322 (2018).
42. Gough, M. J. & Crittenden, M. R. The paradox of radiation and T cells in tumors. *Neoplasia* **31**, 100808 (2022).
43. Shi, X. et al. Mechanism insights and therapeutic intervention of tumor metastasis: latest developments and perspectives. *Signal Transduct. Target Ther.* **9**, 192 (2024).
44. Lee, C. Y. C. et al. Tumour-retained activated CCR7(+) dendritic cells are heterogeneous and regulate local anti-tumour cytolytic activity. *Nat. Commun.* **15**, 682 (2024).
45. Banchereau, J. & Steinman, R. M. Dendritic cells and the control of immunity. *Nature* **392**, 245–252 (1998).
46. Garris, C. S. et al. Successful anti-PD-1 cancer immunotherapy requires T cell-dendritic cell crosstalk involving the cytokines IFN-gamma and IL-12. *Immunity* **49**, 1148–1161.e1147 (2018).
47. D.

48. Sprooten, J., Agostinis, P. & Garg, A. D. Type I interferons and dendritic cells in cancer immunotherapy. *Int. Rev. Cell Mol. Biol.* **348**, 217–262 (2019).
49. Deguine, J. & Barton, G. M. MyD88: a central player in innate immune signaling. *F1000Prime Rep.* **6**, 97 (2014).
50. Zhang, X. et al. The paradoxical role of radiation-induced cGAS-STING signalling network in tumour immunity. *Immunology* **168**, 375–388 (2023).
51. Zhang, L. et al. NF-kappaB activation enhances STING signaling by altering microtubule-mediated STING trafficking. *Cell Rep.* **42**, 112185 (2023).
52. Chen, F. et al. The STING1-MYD88 complex drives ACOD1/IRG1 expression and function in lethal innate immunity. *iScience* **25**, 104561 (2022).
53. Waldman, A. D., Fritz, J. M. & Lenardo, M. J. A guide to cancer immunotherapy: from T cell basic science to clinical practice. *Nat. Rev. Immunol.* **20**, 651–668 (2020).
54. Daguenet, E. et al. Radiation-induced bystander and abscopal effects: important lessons from preclinical models. *Br. J. Cancer* **123**, 339–348 (2020).
55. Dewan, M. Z. et al. Fractionated but not single-dose radiotherapy induces an immune-mediated abscopal effect when combined with anti-CTLA-4 antibody. *Clin. Cancer Res.* **15**, 5379–5388 (2009).
56. Torcellan, T. et al. In vivo photolabeling of tumor-infiltrating cells reveals highly regulated egress of T-cell subsets from tumors. *Proc. Natl Acad. Sci. USA* **114**, 5677–5682 (2017).
57. Sahgal, A. et al. Stereotactic body radiotherapy versus conventional external beam radiotherapy in patients with painful spinal metastases: an open-label, multicentre, randomised, controlled, phase 2/3 trial. *Lancet Oncol.* **22**, 1023–1033 (2021).
58. Wang, J. et al. 323 Immunogenic syngeneic model MC38-OVA for the preclinical evaluation of immune evasion and checkpoint blockade. *J. Immunother. Cancer* **9**, A348–A348 (2021).

Acknowledgements

We thank Dr. Xiaoyu Hu for sharing the MyD88 knockout mice and Dr. Wei Liang for sharing the 4T1-luc2 cells. This work was supported by grants from the National Natural Science Foundation of China (82250710684 to Y.-X.F., 22225603 to Z.L., and 32370967 to W.W.) and the International Postdoctoral Exchange Fellowship Program (to X. Z.).

Author contributions

Conceptualization: X.Y., Y.-X.F., and Z.L.; Methodology: X.Y., Z.D., L.Y., and Y.-X.F.; Investigation: X.Y., Z.D., L.Y., X.Z., Y.G., and Y.L.; Formal analysis: X.Y., Z.D., L.Y., Y.-X.F., and Z.L.; Writing—original draft: X.Y.; Writing—review and editing: X.Y., Z.D., L.Y., and Y.-X.F.; Supervision: Y.-X.F. and Z.L.

Competing interests

The authors declare no competing interests.

Additional information

Supplementary information The online version contains supplementary material available at https://doi.org/10.1038/s41467-025-60769-3.

Correspondence and requests for materials should be addressed to Zhibo Liu or Yang-Xin Fu.

Peer review information *Nature Communications* thanks the anonymous reviewer(s) for their contribution to the peer review of this work. A peer review file is available.